J. Fluid Mech. (1985), *vol.* 161, *pp.* 313–327
Printed in Great Britain

The motion of constant-volume air cavities in long horizontal tubes

By W. D. BAINES,
Department of Mechanical Engineering, University of Toronto, Toronto, Canada M5S 1A4

JAMES W. ROTTMAN AND JOHN E. SIMPSON
Department of Applied Mathematics and Theoretical Physics,
Silver Street, Cambridge CB3 9EW

(Received 16 July 1984 and in revised form 4 July 1985)

Experimental results are presented for the instantaneous release of a constant volume of air into water in a long horizontal tube of square cross-section. The tube is closed at both ends and the volume of air is confined at one of the ends before it is released. The resulting motion, after the rapid formation of an air-cavity front, may be divided into three phases: initially the front of the air cavity moves at constant speed, later its speed decreases monotonically, and finally its speed executes a long series of erratic stops and starts before coming entirely to rest. The transition from the first to the second phase is observed to occur when a disturbance due to the tube end overtakes the cavity front. The final phase is dominated by surface-tension effects, complicated by surface contaminants. A simple model of the flow, based on Benjamin's (1968) theory of steady cavity flow and the classical theory of hydraulic jumps, is developed. With correction for surface tension, the model results compare well with the experimental results for the first two phases.

1. Introduction

Previous experimental studies of air-cavity motion in horizontal tubes have been conducted by Zukoski† (1977), Gardner & Crow (1970) and Wilkinson (1982). In all these investigations, air cavities were produced by opening, fully or partially, one end of a closed tube filled with water. The purpose of the studies described herein was to determine the front speeds and shapes of the air cavities thus produced. The three different kinds of cavity profiles that are observed in tubes of square cross-section are sketched in figure 1.

Benjamin (1968) proposed a theory for such air-cavity motion that assumes the flow is steady and that the effects of surface tension and of viscosity at the solid boundaries are unimportant. By requiring the bulk conservation of mass and momentum in a control volume that moves with the cavity front, he determined the speed of the front as a function of the uniform downstream water depth d and the tube depth D (as shown in figure 1). He also showed that physically possible flows exist only with $d \geqslant \frac{1}{2}D$ and that energy is dissipated in these flows when $d > \frac{1}{2}D$. In addition, he proved that the profile shape for the energy-conserving flow has the shape sketched in figure 1 (a), with the cavity depth asymptotically approaching $\frac{1}{2}D$ downstream.

† Zukoski (1966) also studied cavity motion in inclined tubes and used several liquid–liquid combinations as well as air and water.

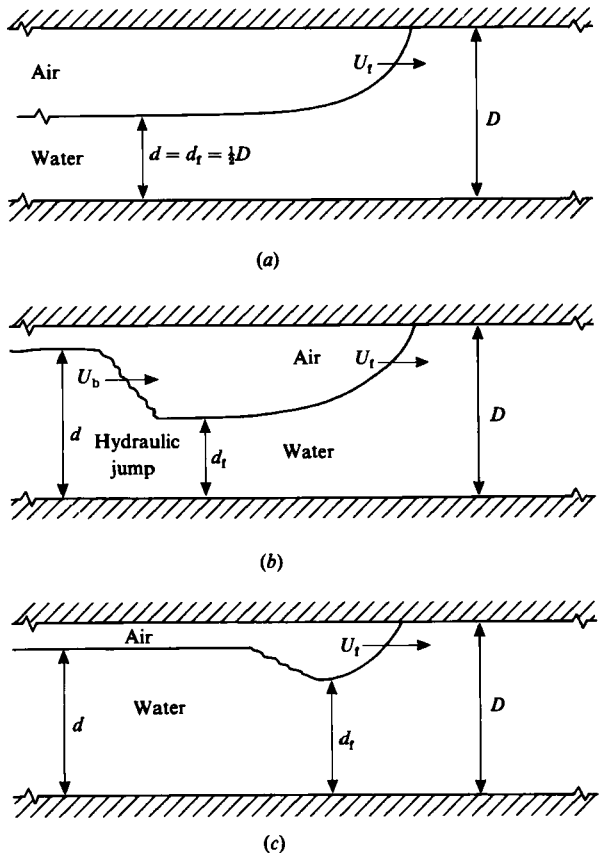

FIGURE 1. The three types of air-cavity profiles observed in experiments in which one end of a water-filled tube is fully or partially removed: (*a*) a smooth steady cavity: (*b*) a smooth cavity front with a downstream hydraulic jump propagating at a speed not equal to the front speed; (*c*) a cavity with a gravity-current-type front.

The observations of the three experimental studies previously cited show that Benjamin's energy-conserving cavity flow results if the water is allowed to flow freely out of the end of the tube – and if the cross-section of the tube is large enough for the effects of surface tension and of the boundary layers at the tube wall to be negligible. However, these effects are significant for normal laboratory tube dimensions. For example, Gardner & Crow's results show that for tube depths of 10 cm the measured front speed is 7 % less than predicted by Benjamin's analysis.

Benjamin suggested that when the water flowing from the end of the tube is throttled, steady flows would probably exist only for $d/D \gtrsim 0.65$ and that the cavities in these flows would have shapes similar to that sketched in figure 1(*c*). He argued that his steady solutions with $0.5 < d/D \lesssim 0.65$ are probably unstable in this experimental arrangement and that they would become unsteady or jump to another steady solution with $0.65 \lesssim d/D \lesssim 0.78$. However, Wilkinson found experimentally that the flow is unsteady if the water depth at the tube outlet is $0.5 < d/D \lesssim 0.78$. The cavity front has the speed and shape of Benjamin's energy-conserving cavity (with $d_f = \frac{1}{2}D$) but is followed by a hydraulic jump (as shown in figure 1*b*) that travels at a speed slower than that of the front. With $d/D > 0.78$ at the water outlet, Wilkinson observed that the flow becomes steady, with cavity shape as shown in

figure 1 (*c*), and the front speed is accurately described by Benjamin's analysis (with small corrections for surface tension).

The work presented herein is an experimental study of the motion that results when an air cavity of constant volume is released from rest in a closed horizontal tube that is filled with water. The purpose of our study is to determine the front speed and shape of the cavity as a function of time after release. Our experimental techniques and qualitative observations are described in §2. The motion after release is in many respects similar to that observed by Wilkinson (1982), but there are some interesting differences which we attempt to model in a new way. In §3, we develop a simple model of the flow, based on Benjamin's (1968) theory – with corrections for surface-tension effects suggested by Wilkinson (1982) – and the classical theory of hydraulic jumps. Finally, in §4, we remark on the implications of our results to two-phase flows in pipes and ducts. We restrict attention to tubes of square cross-section but, following Benjamin (1968), the analysis could readily be adopted to tubes of circular cross-section.

In all our experiments, because of practical necessity, the longitudinal shape of the air cavity before release was a rectangle, but the details of the initial cavity shape should have only a small effect on the resulting motion. We observed in all cases that a steady cavity front is established within a few tenths of a second after release, and that its properties are a function only of the characteristic length and depth of the initial cavity and not of the particular cavity shape. A different initial cavity shape would change only slightly the time taken to establish the steady front. The difference is likely to be smaller than the accuracy with which we could measure the front position.

An application of this flow in engineering practice is the simple horizontal chemical or metallurgical reactor in which a gas volume is released into a cylinder of liquid at rest. The hydraulic jump that occurs in these flows, as we describe later, serves as a mixing zone.

2. Experiments

The experiments were conducted in an acrylic plastic tube of 10 cm square cross-section and 2.5 m length. To contain the volume of air a vertical gate was installed in the tube 40 cm from one end. A moveable wall allowed the length of the tube behind the gate to be reduced if desired. A hand-operated device enabled an operator to withdraw the gate in less than 0.1 s. For an experiment, the tube was partially filled with water while in a tilted position with the gate end slightly raised. The tube was then brought to a horizontal position and the air space behind the gate was adjusted to the desired level by siphoning. The gate was then withdrawn, releasing the air into the tube. The independent parameters in these experiments, then, are the initial cavity length X_0 and the initial depth d_0 of the water under the cavity. All the measurements were taken from still photographs made with a motor-driven camera. An exposure interval of about 0.33 s with accuracy to within 0.02 s was determined from an electronically controlled pattern of lights in each photograph.

The observed motion after release may be divided into several phases. We choose to define the phases primarily according to the behaviour of the cavity front. The cavity front is established within a few tenths of a second after release, and rapidly accelerates up to a constant speed. We call the period during which the front travels at constant speed the first phase. In the following second phase, the front speed

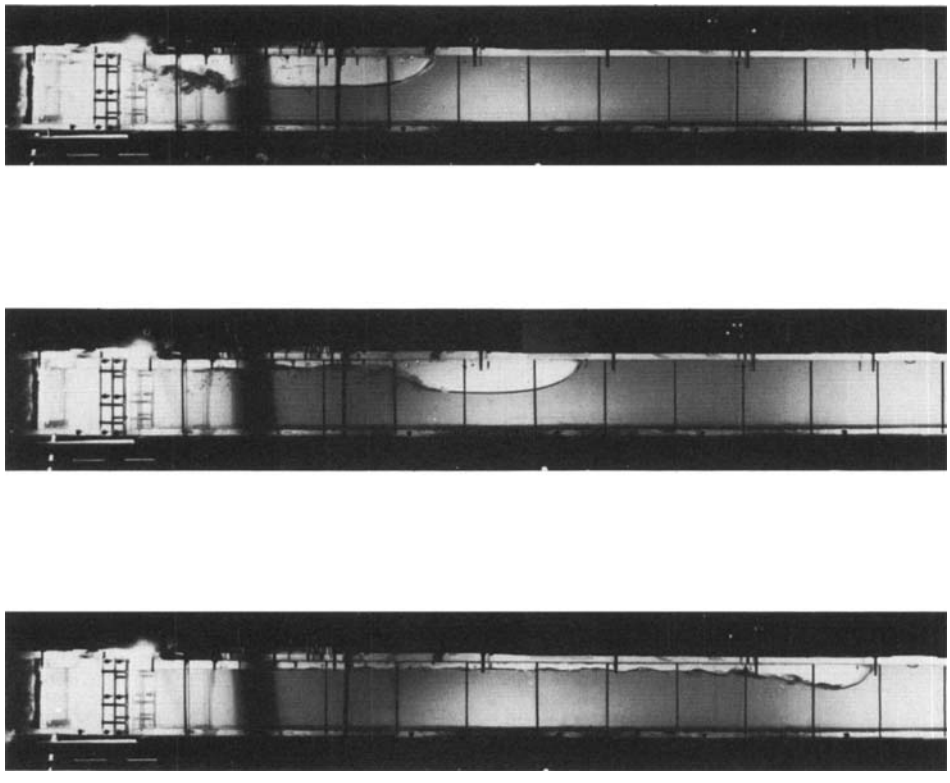

FIGURE 2. Sequential photographs of the collapse of an air cavity at $\frac{2}{3}$, $\frac{4}{3}$ and $\frac{5}{3}$ s after release, with $D = 10$ cm, $d_0 = 0$ cm, $X_0 = 40$ cm. These cavity shapes are representative of cavity flows with $0 \leqslant d_0/D \lesssim 0.3$.

decreases monotonically. Finally, in the third phase, the front executes a long series of erratic stops and starts before coming entirely to rest. The overall shape of the cavity is distinctly different, at least in the first phase of motion, depending on the initial cavity depth.

When $0 \leqslant d_0/D \lesssim 0.3$ the cavity profile in the first phase of motion after release is as shown in the sequential photographs in figure 2. The photographs are actually for the case with $d_0/D = 0$, but they are representative of this class of flows. The overall shape of the cavity, except the front, changes constantly during the first phase. Within a few fractions of a second after release, the front evolves into Benjamin's energy-conserving cavity shape (as in figure 1 *a*). At the same time, the water displaced by the advancing cavity rushes in the opposite direction (toward the end of the tube) in the form of a surge. The overall cavity shape is as shown in figure 2 (*a*). When the surge reaches the tube end it is reflected as a hydraulic jump. The cavity then has the shape shown in figure 2 (*b*). This is similar to what Wilkinson observed, as sketched in figure 1 (*b*), but in the present case, opposite to Wilkinson's observations, the jump has a slightly *greater* speed than that of the cavity front. Eventually the jump overtakes the front, which until this time has maintained constant speed and shape, abruptly reducing its speed and depth, and thus ending the first phase. Just after the jump overtakes the front the shape of the cavity which is shown in figure 2 (*c*) is similar to that in figure 1 (*c*).

When $0.3 \lesssim d_0/D < 1$ the cavity profile in the first phase of motion after release

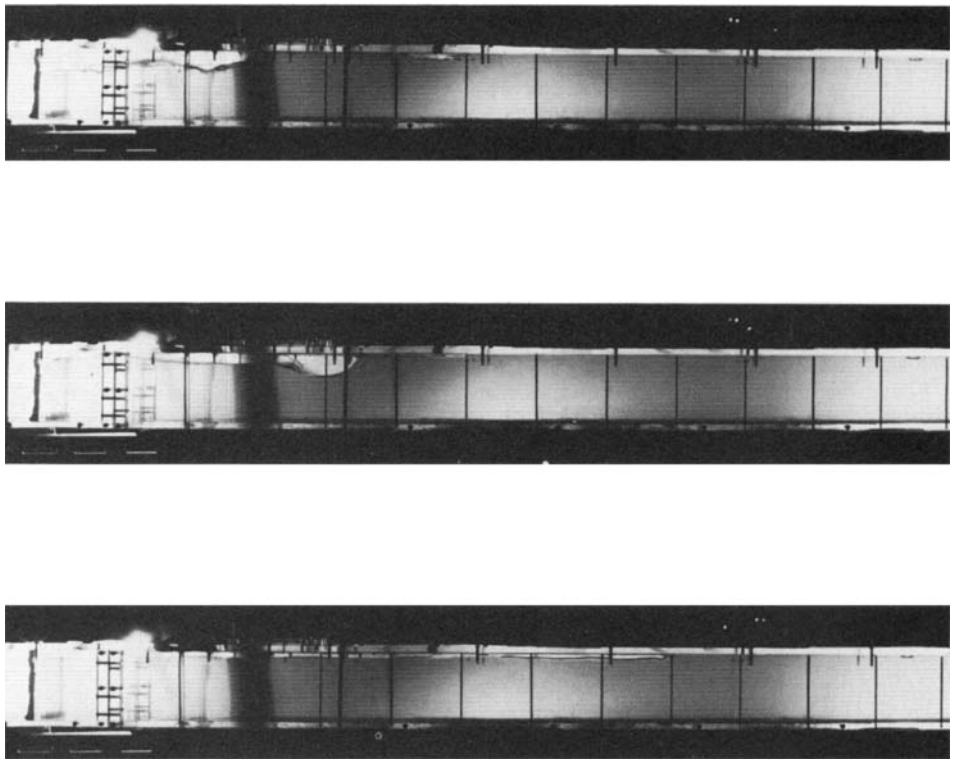

FIGURE 3. Sequential photographs of the collapse of an air cavity at $\frac{1}{3}$, $\frac{2}{3}$ and $\frac{5}{3}$ s after release with $D = 10$ cm, $d_0 = 7$ cm, $X_0 = 40$ cm. These cavity shapes are representative of cavity flows with $0.3 < d_0/D < 1.0$.

is as shown in the sequential photographs in figure 3. Again, although these photographs are actually of the case with $d_0/D = 0.7$, they are representative of this class of flows. As in the previous case, a steady front is formed in a few fractions of a second after release, but here the front consists of a short, rounded bubble that is connected to the following volume of air by a shallow 'neck'. At the same time that this front propagates away from the tube end, what appears to be a weak, undular bore propagates along the bubble interface towards the tube end. The cavity shape at this stage is as shown in figure 3(*a*). The disturbance is reflected at the tube end, producing the cavity shape shown in figure 3(*b*). Eventually the reflected wave overtakes the front, which until this time has maintained constant speed and shape, and the speed and depth of the front begin to decrease. The cavity shape just after this occurs is shown in figure 3(*c*), which is seen to be similar to the profile in figure 2(*c*). A closer look at the cavity front in this case is given in figure 4, which is a superposition of four successive front profiles from one of our experiments. This sequence shows the details of the front being overtaken by the disturbance; we observed that the front speed remained constant until the disturbance reached the part of the cavity where the water depth under the cavity equals d_f (the minimum water depth), then the front speed steadily decreased.

The second and third phases of the motion were qualitatively the same for all the different initial conditions we used. In the second, which begins when the front speed starts to decrease, the cavity is well described as collapsing through a series of

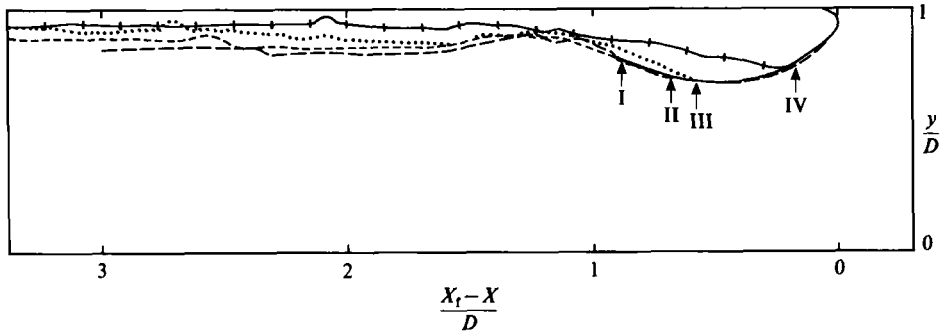

FIGURE 4. Tracings of an air-cavity profile for several times after release with $D = 10$ cm, $d_0 = 7$ cm, $X_0 = 40$ cm. The profiles have been superposed so that the leading edges are at the same position. Roman numerals indicate the position of the leading edge of the disturbance emanating from the tube end. ——I, $t = 0.73$ s; – – – II, $t = 10.04$ s; ... III, $t = 1.37$ s; –|– IV, $t = 1.67$ s.

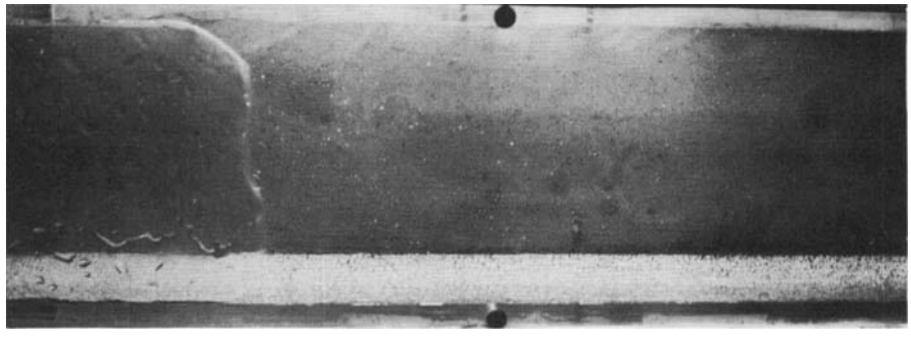

(*a*)

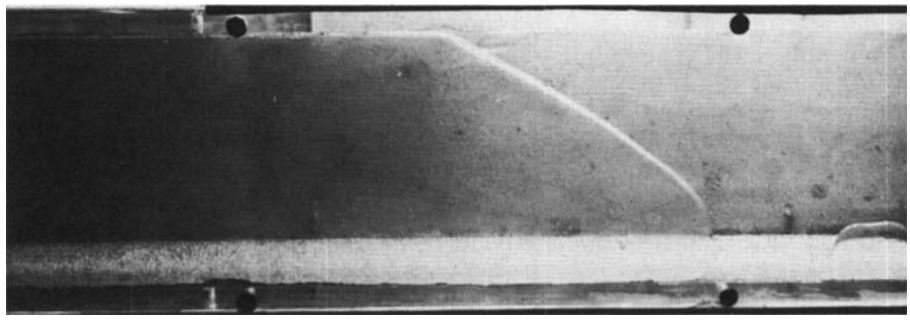

(*b*)

FIGURE 5. Plan-view photographs of the air-cavity front: (*a*) during the second phase; (*b*) during the third phase.

equal-area rectangles, with the front speed and approximately uniform cavity depth decreasing monotonically. In the third phase the cavity front develops an irregular three-dimensional shape and the front speed is erratic. The motion is dominated by surface tension and its effects are complicated by contaminants on the upper tube surface. Figure 5 shows two photographs of the cavity front taken from above the transparent upper surface of the tube. Figure 5(*a*) shows a smooth two-dimensional front during the second phase, and figure 5(*b*) shows an irregular three-dimensional front during the third phase.

Of course the nature of the flow is different if d_0/D is too close to unity or X_0/D is too small. In the first case, surface tension dominates all other effects. The bubble simply jumps to a new equilibrium shape. This appears to occur when $d_0/D \gtrsim 0.8$. In the second case, the formation of the cavity front is interfered with by the end wall. The cavity motion then is a strong function of X_0/D. This appears to occur when $X_0/D \lesssim 1$.

We note in passing that the qualitative features of the first two phases of the collapse of air cavities are similar in many ways to the collapse of a volume of salt water into fresh water, as described by Rottman & Simpson (1983). Quantitatively, the first phase is quite similar, but the second is significantly different. The difference is due mainly to surface tension and the absence of mixing in the air-cavity flows. The final phase, which is dominated by surface tension effects, is of course absent in the salt-water experiments.

3. Results and analysis

3.1. *The first phase*

The two different types of cavity shapes in the first phase are shown schematically in figures 1(*b*) and (*c*). The sketch in figure 1(*b*) corresponds to a flow with $0 \leqslant d_0/D \lesssim 0.3$ and that in figure 1(*c*) to a flow with $0.3 \lesssim d_0/D < 1$, although the depth d in the latter case is not uniform in our flows (as indicated more clearly in figure 4). Even though the cavity shapes are quite different, the front speeds and shapes remain steady during the first phase in both cases.

Figure 6 is a plot of the cavity-front position and the position of the hydraulic jump (after it has been reflected from the tube end), for the flow with $d_0/D = 0$, as functions of time after release. The solid lines in this plot are straight-line fits to the data at early time. It is clear that both the front and the jump travel at constant speed initially and that the front speed begins to decrease at the point where the two straight lines intersect. The speeds of the front and the jump during the first phase were estimated from the slopes of these lines. Similar plots were made for the other values of d_0/D and the estimated speeds thus obtained are plotted in figure 7. For $d_0/D > 0.3$ the disturbance was too weak to measure accurately and so the speeds of these disturbances are not plotted.

The most easily measured characteristic of the cavity front is the minimum water depth d_f, defined in figure 1. This depth is constant in all cases throughout the first phase. For the flows corresponding to figure 1(*b*) the cavity front curves smoothly from its contact line to a level depth d_f. For flows corresponding to figure 1(*c*), the cavity interface is curved where the water depth equals d_f and is rough and unsteady immediately downstream of this point. The other depths that appear in figure 4 are either unsteady or are difficult to measure accurately. The measured values of d_f as a function of d_0/D are plotted in figure 8.

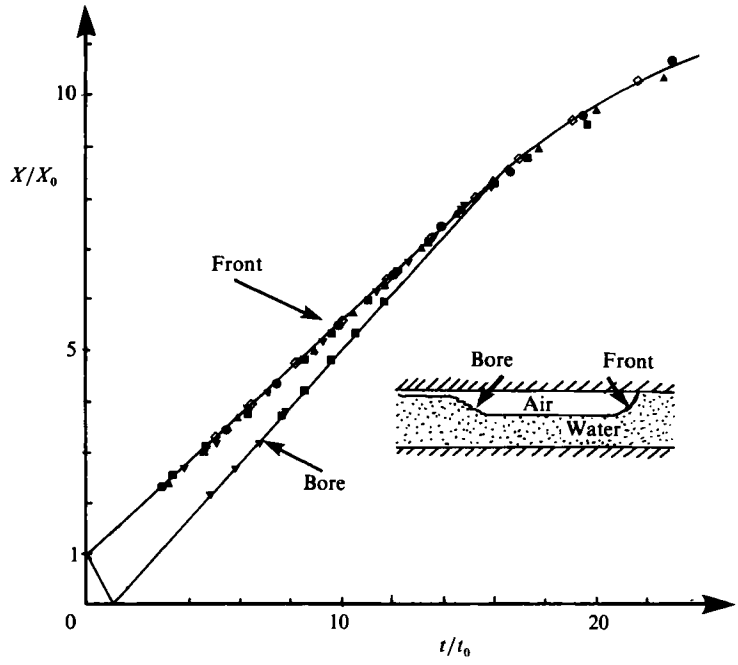

FIGURE 6. The position of the front and the hydraulic jump as a function of time after release for an air cavity with $D = 10$ cm, $d_0 = 0$ cm: —— straight-line fits to the data at early time; ◇, $X_0 = 24$ cm; △, $X_0 = 30$ cm; □, $X_0 = 35$ cm; ▽, $X_0 = 40$ cm.

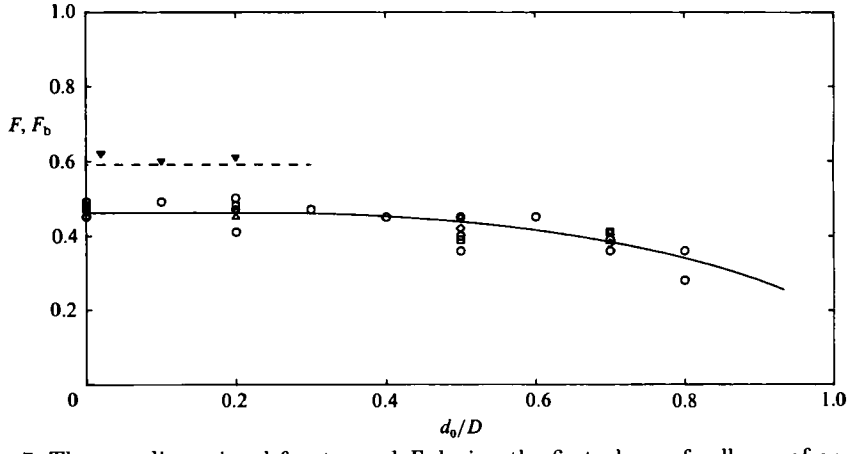

FIGURE 7. The non-dimensional front speed F during the first phase of collapse of an air cavity as a function of d_0/D: ○, $X_0/D = 1$; □, $X_0/D = 2$; ◇, $X_0/D = 3$; △, $X_0/D = 4$. (The solid curve is the solution of (8) and (9).) And the non-dimensional bore speed F_b: ▼. (The dashed line is the theoretical result $F_b = 0.59$.)

We can determine a relationship between the front speed U_f and the depth d_f by using a method similar to that used by Benjamin (1968). Since in general the cavity interface is curved where the water depth equals d_f, we have to modify his method to account for this curvature. We could solve the entire steady-potential-flow problem using the finite-element method developed by Meric, Tubarrok & Baines

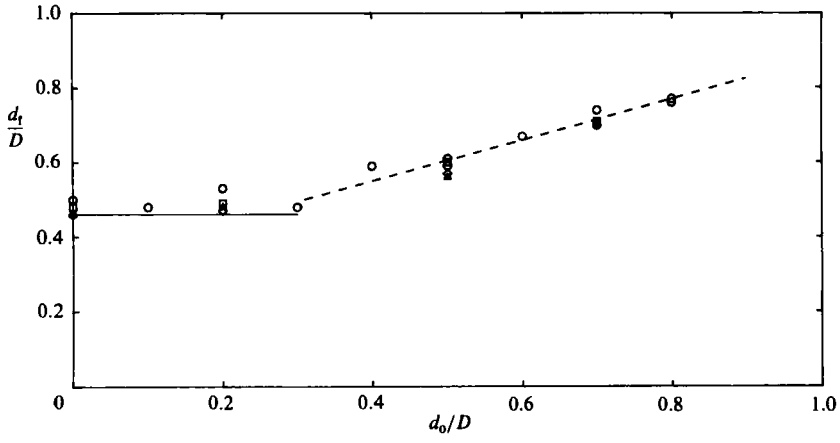

FIGURE 8. The depth d_f of the water under the cavity front during the first phase of collapse of an air cavity as a function of d_0/D. The symbols are as defined in figure 7. The solid line is the value derived in the text for $0 \leqslant d_0/D \lesssim 0.3$, and the dashed curve is a straight-line fit to the data for $0.3 < d_0/D < 1.0$.

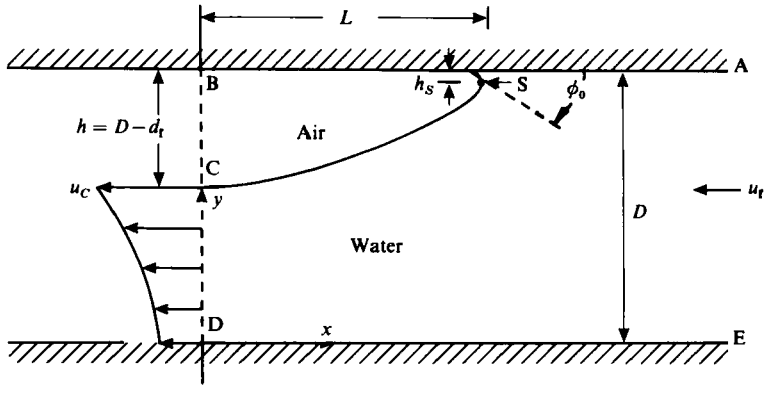

FIGURE 9. Definition sketch for the potential-flow analysis of the air-cavity front.

(1982), but they did not include the effects of surface tension nor of the displacement of the stagnation point due to viscosity. We find the simpler but approximate integral method described below to be entirely adequate for our purposes.

The flow near the cavity front in a reference frame moving with the front is sketched in figure 9. We consider the flow within the control volume ABCDE, as shown in the figure. We have chosen intentionally a region of the flow that is smooth and steady so that, to a good approximation, energy is conserved in the control volume. The conservation equations for the fluxes of mass and momentum are, assuming that the motion is steady and the pressure hydrostatic across AE,

$$\rho U_f D = \rho \bar{u} d_f, \tag{1}$$

$$\rho U_f^2 D + \tfrac{1}{2}\rho g D^2 + p_0 D = \alpha \rho \bar{u}^2 d_f + \tfrac{1}{2}\alpha^1 \rho g d_f^2 + p_1 D, \tag{2}$$

where

$$\bar{u} = \frac{\int_0^{d_f} u \, dy}{d_f}, \tag{3}$$

$$\alpha = \frac{\int_0^{d_f} u^2 \, dy}{\bar{u}^2 d_f}, \tag{4}$$

$$\alpha^1 = \frac{\int_0^{d_f} (p - p_1) \, dy}{\frac{1}{2}\rho g d_f^2}, \tag{5}$$

and p is the pressure in the fluid, p_0 is the pressure at A, p_1 is the pressure in the cavity, g is the acceleration due to gravity and ρ is the density of water (the density of air is considered negligible compared to that of water). If the interface had zero curvature at C (as in Benjamin's model) then $u = \bar{u}$ and $\alpha = \alpha^1 = 1$.

Applying Bernoulli's equation along the streamline ASC and throughout ASCDE, we obtain the relations

$$p_0 + \rho g D + \tfrac{1}{2}\rho U_f^2 + p_C + \rho g d_f + \tfrac{1}{2}\rho u_C^2 = p + \rho g y + \tfrac{1}{2}\rho u^2, \tag{6}$$

where u_C is the fluid speed and p_C is the pressure in the fluid at C. The surface tension and interface curvature at C will cause the pressure in the cavity to exceed the pressure in the fluid such that

$$p_1 = p_C + \frac{\sigma}{r_C}, \tag{7}$$

where σ is the surface tension and r_C the radius of curvature of the interface at C. Using (6) and (7) in (5), we obtain an expression for α^1,

$$\alpha^1 = 1 + F^2 \left(\frac{D}{d_f}\right)^3 \left[\left(\frac{u_C}{\bar{u}}\right)^2 - \alpha\right] - 2\frac{\sigma/r_C}{\rho g d_f}, \tag{8}$$

where $F^2 = U_f^2/(gD)$.

Following Wilkinson (1982) we can also obtain a relationship between p_0 and p_1. We let p_S denote the pressure at the stagnation point S which, due to viscous effects, is located at a distance h_S below the upper boundary (as shown in figure 9). Applying Bernoulli's equation along the streamline AS, we obtain

$$p_0 + \tfrac{1}{2}\rho U_f^2 = p_S - \rho g h_S. \tag{9}$$

The relationship between the pressure inside the cavity and the stagnation pressure is

$$p_1 = p_S + \sigma/r_S, \tag{10}$$

where r_S is the radius of curvature of the interface at S. From (9) and (10) we obtain the desired relationship

$$p_1 = p_0 + \tfrac{1}{2}\rho U_f^2 + \sigma/r_S + \rho g h_S. \tag{11}$$

Using (1), (7), (8) and (9) in (2) and (6), we obtain the two equations

$$F^2 + 1 = F^2 \frac{D}{d_f}\left[\alpha + \left(\frac{u_C}{\bar{u}}\right)^2\right] + \left(\frac{d_f}{D}\right)^2 - 2\frac{a^2}{r_C D}\left(\frac{d_f}{D}\right) + \Delta, \tag{12}$$

$$2 = F^2 \left(\frac{D}{d_f}\right)^2 \left(\frac{u_0}{\bar{u}}\right)^2 + 2\left(\frac{d_f}{D}\right) - 2\frac{a^2}{r_C D} + \Delta, \tag{13}$$

where $a = \sigma/(\rho g)$ and $\Delta = 2a^2/(r_S D) + 2h_S/D$.

Equations (12) and (13) are the same as those derived by Wilkinson (1982) if we set $\alpha = 1$, $(u_C/\bar{u}) = 1$ and $r_C = \infty$; that is, the equations are the same as Wilkinson's if we neglect the effects of interface curvature at C. As did Wilkinson, we have neglected the contribution to these equations due to surface tension that Gardner & Crow (1970) included. These terms are of order $(a/D)^2$, and for our size tubes are much less than the included surface-tension effects which are of order $a^2/(r_S D)$. In the following, we also neglect the terms in (12) and (13) that are of order $a^2/(r_C D)$, because these are also generally much smaller than the surface-tension terms of order $a^2/(r_S D)$. This assumption is verified by the calculations of Meric *et al.* (1982).

Wilkinson's 1982 experiments show that the shape and dimensions of a *moving* cavity in the immediate neighbourhood of the stagnation point are approximately independent of the speed of the cavity front. The parameter Δ is only dependent on the shape of the cavity near the stagnation point, and the value that Wilkinson proposed for this parameter is $\Delta \approx 2.8a/D$. The numerical calculations of two-dimensional bubbles by Meric *et al.* (1982) suggest that, to a good approximation, $\alpha + (u_C/\bar{u})^2 \simeq 1 + (u_C/\bar{u})^2$ in (12). With these assumptions, (12) and (13) determine F and d_f/D for specified $u_C/\bar{u}$. Note that the range is $1.0 \leqslant u_C/\bar{u} \lesssim 1.6$.

For flows with $0 \leqslant d_0/D \lesssim 0.3$, the cavity interface is smooth and asymptotically becomes level downstream. The appropriate value of $(u_C/\bar{u})^2$ for this case is unity. Substituting this value in (12) and (13), we retrieve Wilkinson's (1982) result

$$\frac{d_f}{D} = F = \tfrac{1}{2}(1-\Delta). \tag{14}$$

If we set $\Delta = 0$ in this expression, we obtain Benjamin's (1968) result for his energy-conserving cavity. With $\Delta = 0.08$, which is the appropriate value for an air–water interface at 20 °C in our 10 cm deep tube $d_f/D = F = 0.46$, in good agreement with our measurements as shown in figures 7 and 8.

For $1 > d_0/D \gtrsim 0.3$, the relationship between F and d_f/D from (12) and (13) is compared with our measured values in figure 7. To obtain this comparison, we used the relation

$$\frac{d_f}{D} = 0.33 + 0.55\frac{d_0}{D}, \tag{15}$$

which is obtained by fitting a straight line to the data points between $1 > d_0/D \gtrsim 0.3$ in figure 8, and the parameter $(u_C/\bar{u})$ was varied from 1.0 to 1.6. The results plotted in figure 7 show the agreement between the theory and the measurements.

When $0 \leqslant d_0/D \lesssim 0.3$, the hydraulic jump that is generated at the tube end and which eventually overtakes the cavity front is well defined and easy to measure. Since the free surface is level and steady on either side of the jump, its speed and strength can be simply estimated using classical theory. The water is at rest relative to the tube downstream of the jump, so mass conservation through the jump requires

$$U_b(d-d_f) = U_f(D-d_f), \tag{16}$$

where U_b is the speed of the jump (or bore), and conservation of momentum through the jump gives the additional relation

$$\left(\frac{d}{d_f}\right)^3 - \left(\frac{d}{d_f}\right)^2 - b\left(\frac{d}{d_f}\right) + 1 = 0, \tag{17}$$

where $b = 1 + 2F^2D(D-d_f)^2/d_f^3$ is a constant defined by the speed and depth of the front. If the ideal front derived by Benjamin (1968) is used, we find that the only

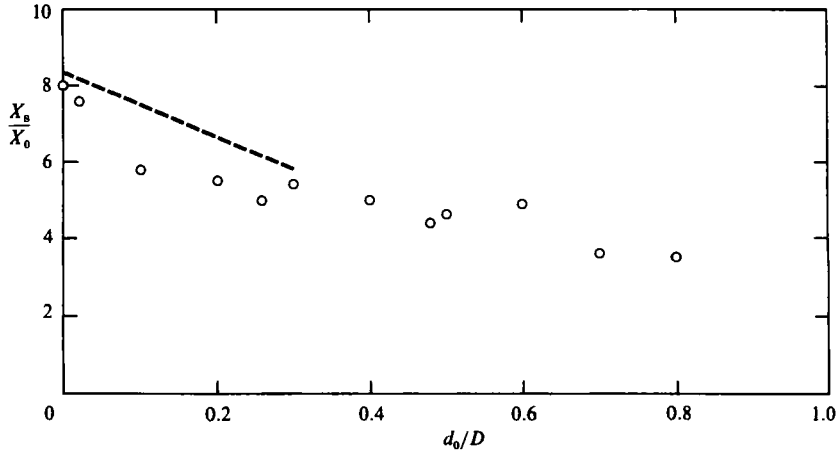

FIGURE 10. The length X_S of the cavity when its front speed begins to decrease, as a function of d_0/D: ---, theory; O, experiment, as computed from (15).

valid solution of (16) and (17) is $d/D = 0.90$ and $F_b = U_b/gD)^{\frac{1}{2}} = 0.62$ and, if the corrections of Wilkinson (1982) are applied, the solution is $d/D = 0.886$, $F_b = 0.59$. The average value of d/D from 13 experiments with uniform flow underneath the cavity is 0.885 ± 0.015, in close agreement with the theoretical value. The solution for F_b is plotted with the measured values in figure 7 and is also in good agreement. We note that this particular cavity solution is one member of a set of cavities determined by Wilkinson (1982).

3.2. *The second phase*

Since the cavity shape is observed to be approximately rectangular at the beginning of the second phase, an estimate of the position X_s of the cavity front and of the time t_s after release at which the second phase begins, are given by

$$X_s = X_0(D-d_0)/(D-d_s), \tag{18}$$

$$t_s = (X_s - X_0)/U_f, \tag{19}$$

where d_s is the (approximately uniform) depth of the water under the cavity at the beginning of the second phase. Relations (18) and (19) follow from the conservation of the cavity volume and the steadiness of the front speed during the first phase. For the cases with $0 \leqslant d_0/D \lesssim 0.3$, $d_s/D = 0.886$, as derived above. The value of X_s/X_0 from (18) using this value for d_s/D is plotted in figure 10 as a function of d_0/D. Also shown in this plot are our measurements of this length. The measurements were made by determining the position on a plot of the front position versus time where the deviates form a straight line. For $d_0/D > 0.3$ we have no theoretical estimates of d_s/d_0, but it appears from the data in figure 10 that X_s/X_0 does not vary much from about 4 in these cases.

During the second phase of collapse the depth of the front (or leading edge) of the cavity is only slightly larger than the nearly horizontal surface of the remainder of the cavity. Therefore it is reasonable to approximate the profile as rectangular. Thus, conservation of air volume can be written

$$\frac{X_0(D-d_0)}{(D-d)}\dot{d} = (D-d)\,U_f, \tag{20}$$

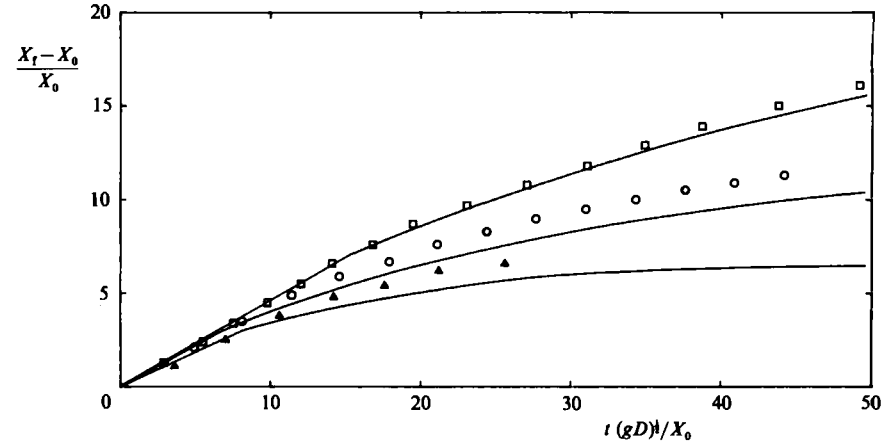

FIGURE 11. The cavity-front position as a function of time after release. Experiments: □, $d_0/D = 0$; ○, $d_0/D = 0.5$; △, $d_0/D = 0.7$. Theory: —— (numerical solution of (17)).

where d is the uniform depth of the water under the cavity and the overhead dot denotes differentiation with respect to time. Furthermore, if we assume that the front speed is quasi-steady, then conservation of momentum for the flow relative to the cavity is expressed by (1) with $\alpha = 1$ and $u_C/\bar{u} = 1$. The front speed U_f therefore can be determined from (12) as a function of d/D. Here we have chosen the section CD sufficiently far behind the front so that the surface is level and consequently we can no longer require the conservation of energy. Substituting this relation for u_f into (20), we obtain a differential equation for d as a function of time

$$\frac{X_0}{(gD)^{\frac{1}{2}}}\dot{d} = \frac{(D-d)^2}{(D-d_0)}\left[\frac{d}{D^2}(D^2-d^2-\Delta D^2)/(2D-d)\right]^{\frac{1}{2}}. \tag{21}$$

Numerical solutions of this equation are plotted in figure 11 along with our experimental measurements for these particular cases. The initial conditions for (21) were obtained from figures 9 and 10 and (9). The data plotted in this figure are measurements of the front position X_f as a function of time after release. The front position is related to d in (21) by $X_f(D-d) = X_0(D-d_0)$. The agreement is seen to be good.

3.3. *The third phase*

The third phase begins when the cavity motion becomes erratic. This occurs because the surface-tension forces become strong enough to bring the motion to rest; that is, the cavity approaches the limit of a static two-dimensional bubble. The value of Δ in the static limit is different from the value we have used for the moving cavity. For a stationary bubble, $h_S = 0$ and r_S depends in some way on the contact angle between the air–water interface and the solid surface. The motion is erratic because randomly distributed contaminants on the Plexiglas surface affect the contact angle.

We can estimate the length of a static two-dimensional cavity with specified contact angle ϕ_0 (see figure 9) in the following way. For a bubble of infinite length, the interface becomes plane far from the contact point. The maximum depth h of such a bubble, as derived (for example) by Batchelor (1967 pp. 63–68), is

$$h = D-d = [2a^2(1+\cos\phi_0)]^{\frac{1}{2}}. \tag{22}$$

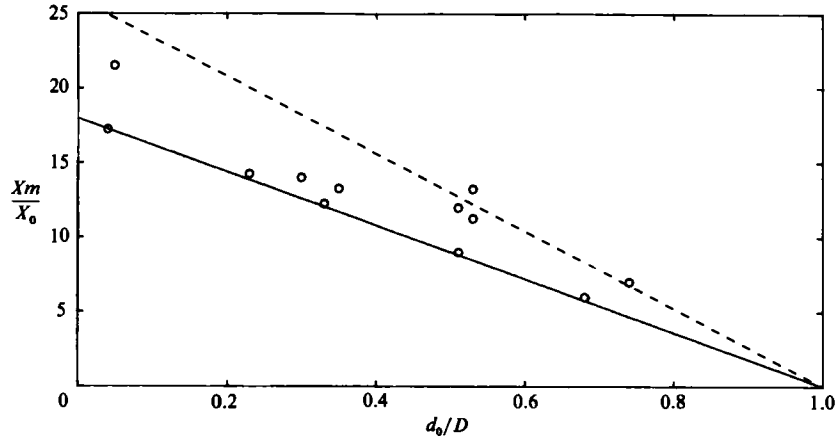

FIGURE 12. The measured lengths of air cavities at the time when the front motion becomes erratic (the beginning of the third phase). The predicted lengths from (19): ——, contact angle = 0; ---, contact angle = 90°.

The bubbles in our experiments were not infinite, but had a length at least 100 times the depth, so the interface is nearly plane far from the contact point and (18) is a very good estimate for h. The static length Xm of our bubbles, then, can be obtained from the conservation of bubble volume as

$$Xm = \left[2\frac{a^2}{D^2}(1+\cos\phi_0)\right]^{\frac{1}{2}}\left(1-\frac{d_0}{D}\right)X_0. \tag{23}$$

For an air–water–Plexiglas interface, $\phi_0 = 0$, and for an air–water interface at 20 °C in our 10 cm tube, $a/D = 0.027$. With these volumes, the static bubble length is $Xm \simeq 18(1-d_0/D)X_0$. If the surface is contaminated, ϕ_0 would be increased. Taking $\phi_0 = \frac{1}{2}\pi$, the maximum value expected for a contaminated surface, $Xm \simeq 26(1-d_0/D)X_0$.

A series of twelve experiments was carried out in which the value of Xm was measured. The value of Xm was taken as the length of the bubble just before its motion became erratic. The results are plotted in figure 12. The solid line in the figure is (19) with $\phi_0 = 0$ and dashed line with $\phi_0 = \frac{1}{2}\pi$. No attempt was made to remove contaminants from the surface, so a random distribution of values of ϕ_0 between 0 and $\frac{1}{2}\pi$ would be expected. This is confirmed by the experimental results falling between the lines.

4. Concluding remarks

The characteristic bubble behaviour that we have described has also been seen for large air bubbles in more complicated flows. The photographs made by Fuentes (1969), for example, of large bubbles being transported through a circular pipe, clearly show the type of behaviour we would expect from our experiments. The techniques we have used should be able to predict other features of this flow and should provide a basis for analysis of other two-phase flows.

REFERENCES

BATCHELOR, G. K. 1967 *Introduction to Fluid Dynamics*. Cambridge University Press.

BENJAMIN, T. B. 1968 Gravity currents and related phenomena. *J. Fluid Mech.* **31**, 209–248.

FUENTES, R. 1969 Contribution à l'étude d'une bulle d'air en mouvement dans l'eau sous une paroi. Thèse de docteur d'université, Grenoble.

GARDNER, C. G. & CROW, I. G. 1970 The motion of large air bubbles in horizontal channels. *J. Fluid Mech.* **43**, 247–255.

MERIC, R. A., TUBARROK, B. & BAINES, W. D. 1982 Finite element analysis of finite gravity surges. *Proc. 4th Intl Symp. on Finite Elements in Flow Problems*, pp. 487–494. University of Tokyo Press.

ROTTMAN, J. W. & SIMPSON, J. E. 1983 Gravity currents produced by instantaneous release of a heavy fluid in a rectangular channel. *J. Fluid Mech.* **135**, 95–110.

WILKINSON, D. L. 1982 Motion of air cavities in long horizontal ducts. *J. Fluid Mech.* **118**, 109–122.

ZUKOSKI, E. E. 1966 Influence of viscosity, surface tension and inclination angle on motion of long bubbles in closed tubes. *J. Fluid Mech.* **25**, 821–840.